Bioconjugate Chemistry

Article

pubs.acs.org/bc

Folate Receptor-Mediated Enhanced and Specific Delivery of Far-Red Light-Activatable Prodrugs of Combretastatin A-4 to FR-Positive Tumor

Gregory Nkepang,[†] Moses Bio,[†] Pallavi Rajaputra,[†] Samuel G. Awuah,[†] and Youngjae You*[,†,‡]

[†]Department of Pharmaceutical Sciences, College of Pharmacy, University of Oklahoma Health Sciences Center, Oklahoma City, Oklahoma 73117, United States

[‡]Department of Chemistry and Biochemistry, University of Oklahoma, Norman, Oklahoma 73019, United States

Supporting Information

ABSTRACT: We examined the concept of a novel prodrug strategy in which anticancer drug can be locally released by visible/near IR light, taking advantage of the photodynamic process and photo-unclick chemistry. Our most recently formulated prodrug of combretastatin A-4, Pc-(L-CA4)$_2$, showed multifunctionality for fluorescence imaging, light-activated drug release, and the combined effects of PDT and local chemotherapy. In this formulation, L is a singlet oxygen cleavable linker. Here, we advanced this multifunctional prodrug by adding a tumor-targeting group, folic acid (FA). We designed and prepared four FA-conjugated prodrugs **1**−**4** (CA4-L-Pc-PEG$_n$-FA: n = 0, 2, 18, ∼45) and one non-FA-conjugated prodrug **5** (CA4-L-Pc-PEG$_{18}$-boc). Prodrugs **3** and **4** had a longer PEG spacer and showed higher hydrophilicity, enhanced uptake to colon 26 cells via FR-mediated mechanisms, and more specific localization to SC colon 26 tumors in Balb/c mice than prodrugs **1** and **2**. Prodrug **4** also showed higher and more specific uptake to tumors, resulting in selective tumor damage and more effective antitumor efficacy than non-FA-conjugated prodrug **5**. FR-mediated targeting seemed to be an effective strategy to spare normal tissues surrounding tumors in the illuminated area during treatment with this prodrug.

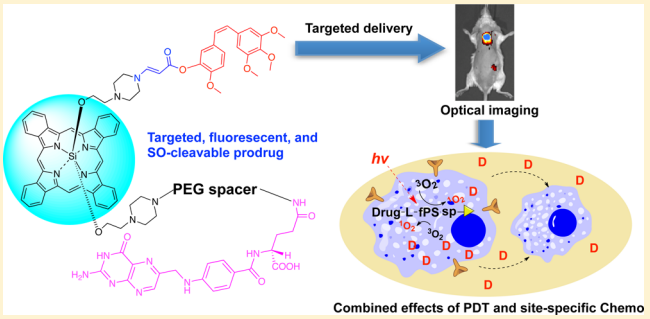

INTRODUCTION

Chemotherapy is one of the major tools to treat both localized and metastasized cancers, and has been used for more than 50 years. However, the problem of systemic side effects resulting from chemotherapy is still unsolved. A more effective drug delivery system could minimize the systemic side effects of anticancer drugs, particularly when such a system meets two goals: tumor-specific delivery and tumor-specific release of drugs from delivery systems.[1−3] While many effective targeting methods, such as liposome-, polymer-, and antibody-based delivery systems have been incorporated into preclinical or clinical use,[4−14] more effective methods for controlling the site of drug release have yet to be developed. Most stimuli that have been exploited to release free drugs from the delivery systems are endogenous.[1,15,16]

Light has been recognized as an excellent external stimulus for spatiotemporal control of drug release from various drug delivery forms, such as prodrugs, liposomes, polymers, and other nano- and macro-delivery systems.[17] The use of longer visible and NIR light is desirable for treating bulk solid tumors because these types of light can reach deeper tissues. However, there is an unfilled gap between such low-energy light and its ability to trigger the cleavage reactions of the chemical bond (linker) that is often required to release the drugs. We proposed a novel drug activation/release strategy, based on photodynamic processes and the unique chemistry of singlet oxygen to spatiotemporally control the release of drugs using visible or NIR light.[18−29] This strategy takes advantage of spontaneous cleavage of dioxetanes that were formed via the [2 + 2] cycloaddition reaction of the singlet oxygen formed during photodynamic processes with electron-rich olefins.

Our previous work on the visible/NIR light-controlled site-specific activation of prodrugs using a photodynamic process led to discovery of the aminoacrylate bond as an ideal linker for singlet oxygen (SO)-cleavable drug release.[18,26] We call this method of drug release "photo-unclick chemistry". We unambiguously proved the novel concept of visible/near IR light-controlled and SO-mediated activation of prodrugs using both in vitro and in vivo models.[19,20] Specifically, we demonstrated far-red light-activated, SO-mediated drug release from two prodrugs of combretastatin A-4 (CA-4), CMP-L-CA4, and Pc-(L-CA4)$_2$ (Figure 1). Our study showed combined effects from photodynamic damage and local chemotherapy, and bystander effects from the released CA4

Received: August 14, 2014
Revised: October 12, 2014
Published: October 28, 2014

   dx.doi.org/10.1021/bc500376j | *Bioconjugate Chem.* 2014, 25, 2175−2188

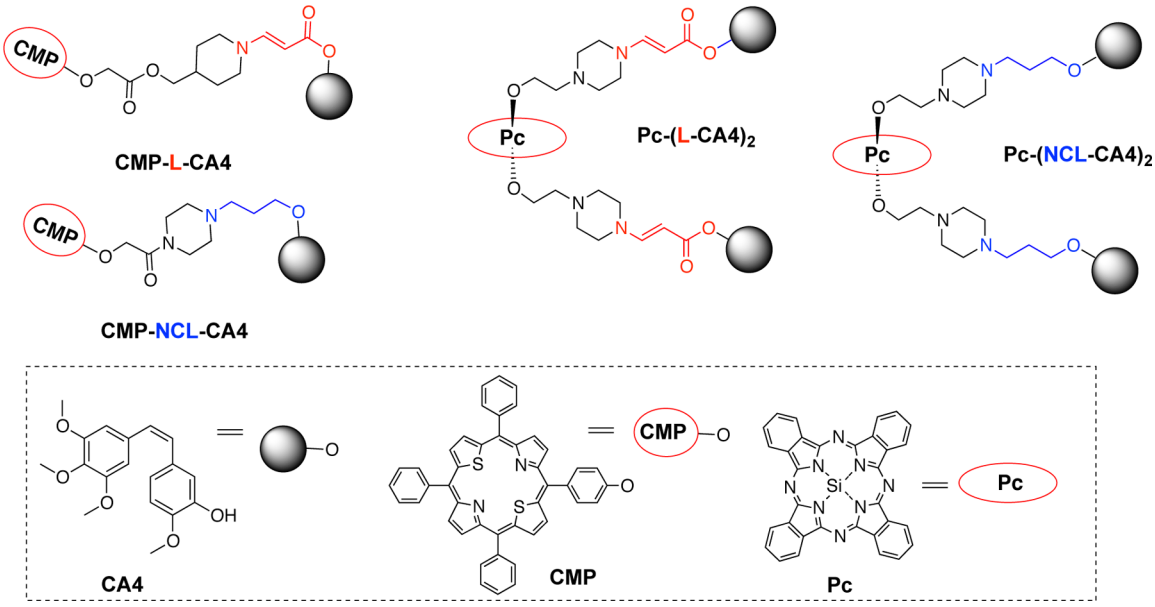

Figure 1. Structures of nontargeted SO-labile prodrugs of CA4 [CMP-L-CA4 and Pc-(L-CA4)$_2$] and their corresponding noncleavable prodrugs [CMP-NCL-CA4 and Pc-(NCL-CA4)$_2$].[19,20]

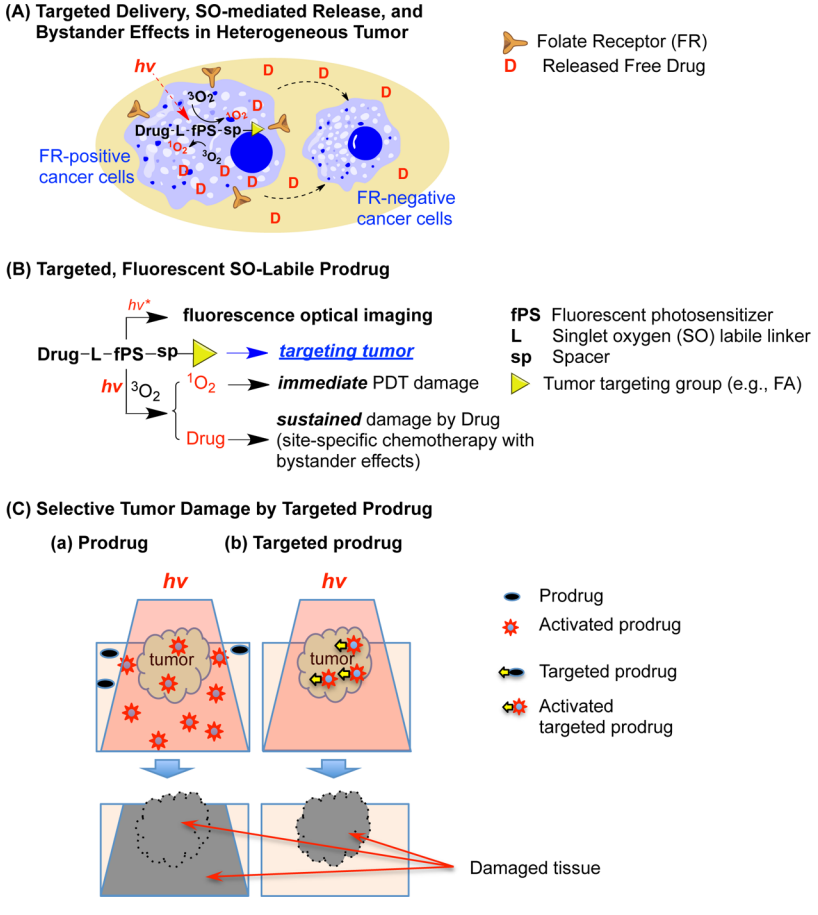

Figure 2. (A) FR-mediated uptake, light-controlled activation, and bystander effects in tumors. Bystander effects from the released drugs can effectively kill the cancer cells that survive after PDT damage. (B) Targeted, fluorescent SO-cleavable prodrug for optical imaging and synergistic combination therapy of PDT and site-specific chemotherapy. (C) Selective tumor damage by targeted prodrug. Unlike nontargeted prodrugs (a), targeted prodrugs will minimize collateral damage to the normal tissue surrounding tumors.

(Figure 2A). Because the lifetime of SO is short (submicrosecond scale), SO as an effector of PDT itself cannot cause bystander effects during the illumination. While bystander effect in PDT by the secondary oxidative product like H_2O_2 has been observed,[30,31] bystander effect in this manuscript focus on that caused by the released chemotherapy drugs.

dx.doi.org/10.1021/bc500376j | Bioconjugate Chem. 2014, 25, 2175−2188

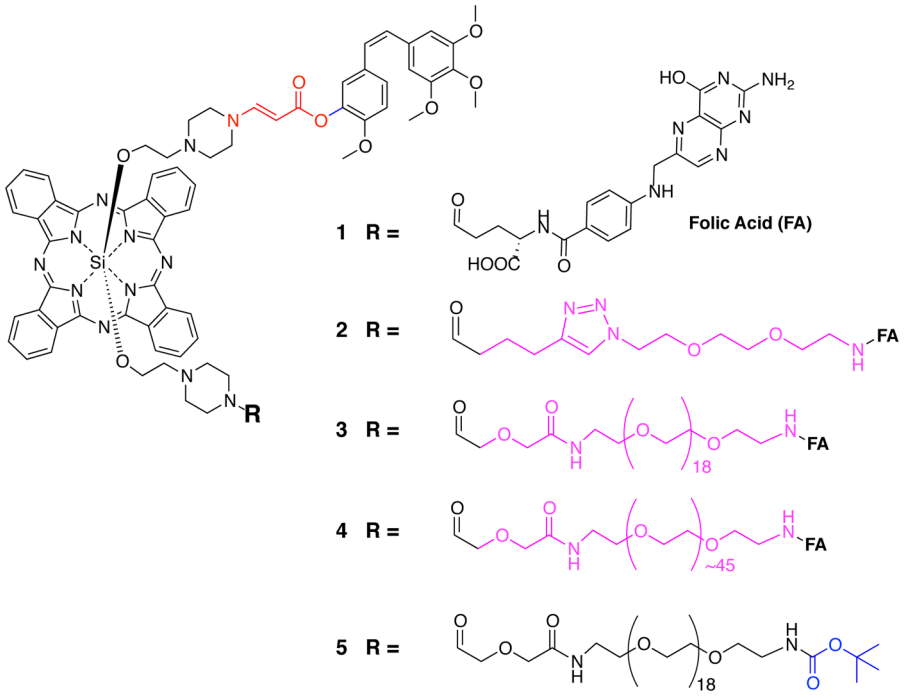

Figure 3. Structures of targeted prodrugs **1**–**4** and nontargeted prodrug **5**.

Scheme 1. Synthetic Routes of Prodrugs 1–5[a]

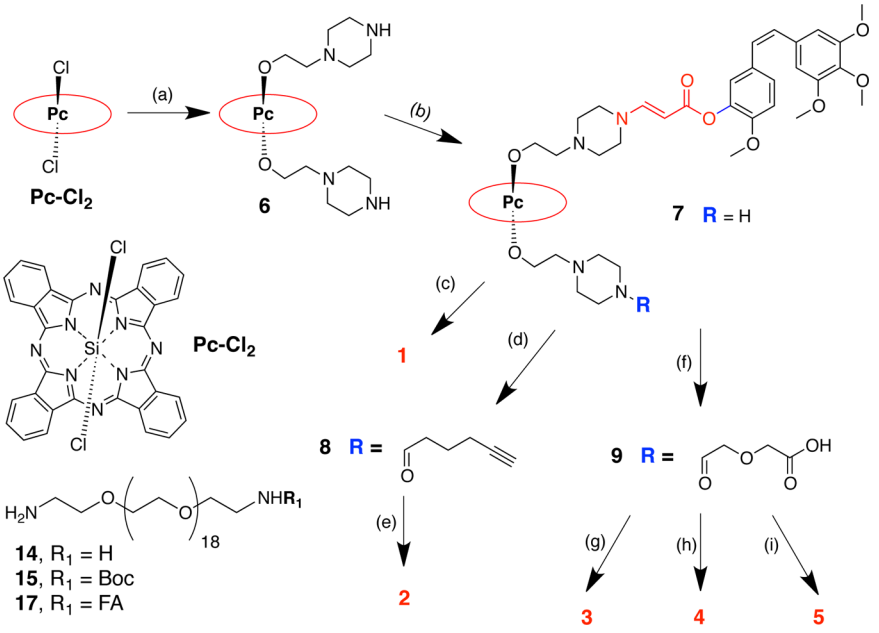

[a]Reaction conditions and reagents: (a) Pc-Cl_2, 1-(2-hydroxyethyl)piperazine, reflux, toluene/pyridine (39:1 v/v), overnight, 76% yield. (b) **6** (1 equiv), CA4 propiolate (1 equiv), THF, rt, 1 h, 58% yield. (c) (i) **FA** (1 equiv), DCC (6.2 equiv), DMF/pyridine (5:1 v/v), sonicate, 30 min; (ii) add **7** (1 equiv), rt, 24 h; (iii) precipitate in cold Et_2O/acetone (3:1 v/v), (iv) dialysis, 48 h, 62% yield. (d) **7** (1 equiv), 5-hexynoic acid (2 equiv), HBTU (2 equiv), DIPEA (4 equiv), DCM (4 mL), rt, 1 h, 81% yield. (e) (i) **8** (1 equiv), **13** (1 equiv), CuBr (1 equiv), PMDETA (1 equiv), 37 °C, DMF (2 mL), 48 h; (ii) Dialysis, 72 h, 60% yield. (f) **7** (1 equiv), diglycolic anhydride (1 equiv), rt, DMF (6 mL), 36 h, 69% yield. (g) **9** (1 equiv), **17** (1 equiv), HBTU (1.5 equiv), DIPEA (3 equiv), rt, DMF (4 mL) overnight, 63% (h) **9** (1 equiv), NH_2–$PEG_{\sim 45}$–FA (1 equiv), HBTU (1.5 equiv), DIPEA (3 equiv), rt, DMF (4 mL) overnight, ~58% yield. (i) **9** (1 equiv), **15** (1 equiv), HBTU (1.5 equiv), DIPEA (3 equiv), rt, DMF (4 mL) overnight, 74% yield.

In the CA4 prodrugs, L is the SO-labile linker and core-modified porphyrin (CMP) and phthalocyanine (Pc) are photosensitizers. Pc-$(L\text{-}CA4)_2$ could be optically imaged in mice due to the bright emission from the fluorescent photosensitizer (fPS), Pc. These two prodrugs showed significantly better antitumor effects than their corresponding noncleavable prodrugs, CMP-NCL-CA4 and Pc-$(NCL\text{-}CA4)_2$, in which NCL refers to the noncleavable linker. These prodrugs were designed to maximize the antitumor efficacy while minimizing the side effects. Interestingly, the prodrug CMP-

dx.doi.org/10.1021/bc500376j | *Bioconjugate Chem.* 2014, 25, 2175–2188

Table 1. Electronic Absorption in DMF and log $D_{7.4}$ Values for Prodrugs 1−5

compounds	λ_{max} (nm) (log ε)				log $D_{7.4}$
1	675 (5.20)	646 (4.40)	607 (4.45)	355 (4.93)	0.84
2	675 (5.35)	646 (4.53)	607 (4.60)	355 (4.99)	1.13
3	675 (5.33)	646 (4.46)	607 (4.53)	355 (4.89)	−0.05
4	675 (5.39)	646 (4.57)	607 (4.63)	355 (5.00)	−0.12
5	675 (5.30)	646 (4.46)	607 (4.60)	355 (4.86)	0.65

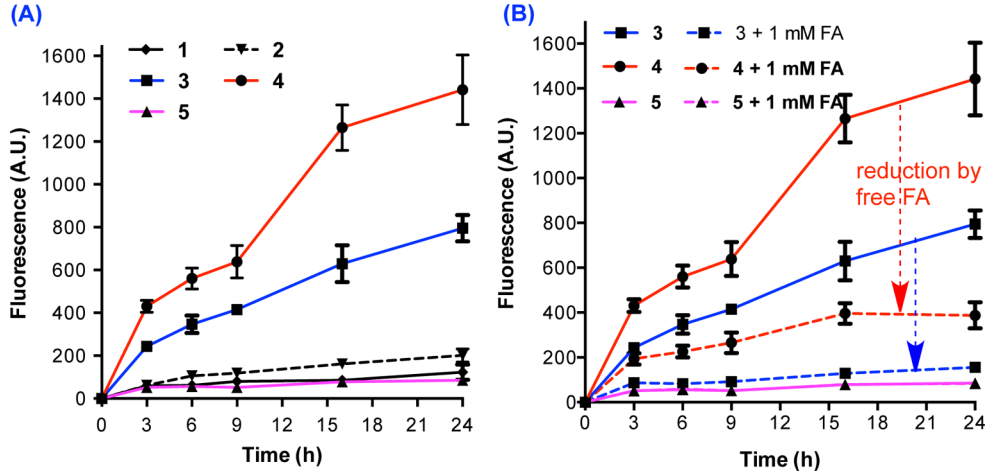

Figure 4. (A) Time-dependent cellular uptake of prodrugs **1**−**5**. Colon 26 cells were incubated with 10 μM prodrugs. At various time points, the prodrugs in the cells were quantified by fluorescence emitted from Pc of the prodrugs. (B) Impact of excess free FA on the cellular uptake of the prodrugs. Cells were pretreated (1 h) with 1 mM free FA before the addition of 10 μM of prodrugs **3**, **4**, and **5**. The prodrugs in cells were quantified in the same way as in (A). Data are means ± SD (n = 3).

L-CA4 showed a significantly superior antitumor effect as opposed to a simple combination of PDT (CMP-NCL-CA4) and chemotherapy (CA4) without systemic side effects.[19]

Here, we advance our novel light activatable prodrug strategy by adding a tumor-targeting group to the prodrug system (Figure 2A). Optical imaging can also monitor the prodrugs (Figure 2B). The dose of light required for fluorescence imaging is much lower than what is needed for drug release; therefore, we do not expect that imaging causes significant tumor damage. We hypothesized that by using a tumor-specific delivery vector such as folic acid (FA), we could selectively deliver the prodrugs to folate receptor (FR)-overexpressing cancer cells and tumors, and thus minimize the collateral damage to normal tissues after broader illumination (Figure 2C). We present four targeted prodrugs (**1**−**4**) and one nontargeted prodrug (**5**), as a control. The four prodrugs were designed with different spacer lengths (Figure 2B), because we assumed that the length of the spacer is a major factor for effective binding of FA-conjugate and FR. In this paper, we discuss the design and synthesis of these prodrugs, in vitro cellular uptake to FR-positive colon 26 cells, the impact of free folic acid on uptake, in vitro phototoxicity, uptake to colon 26 tumors on mice, and specific tumor damage from treatment with the selected prodrugs.

RESULTS AND DISCUSSION

Design and Synthesis of Prodrugs. The general prodrug structure of CA4-L-Pc-sp-FA was designed based on our previous nontargeted fluorescent prodrug, Pc-(L-CA4)$_2$, in which one of the CA4 units was used as a targeting group (Figure 2B and Figure 3). We chose folic acid (FA) because the folate receptor (FR), a glycosylphosphatidylinositol-linked membrane protein, is a well-known tumor-associated receptor that is overexpressed in many tumors, including ovarian, lung, colon, and breast cancers.[9,32−34] FA[35] or FA conjugates[36] can also be taken up preferentially by cancer cells; thus, folate−drug conjugates have been developed and tested in cultures, animal models, and human clinical trials with successful results.[9,37−44]

PEG was chosen as a spacer group because it is FDA-approved, hydrophilic, and biocompatible. PEG conjugation to our prodrugs would increase solubility, thereby reducing the aggregation and nonspecific uptake of the resulting conjugates by the cells or tumors, as well as increasing the targeting capability.[45−47] The prodrugs' PEG length was varied, because spacer length was one of the major factors for FA-targeting efficiency.[48−52] Prodrug **5** was designed as a nontargeted prodrug that was similar to its targeted counterpart (**3**), but would serve as a control to assess the contribution of FA to the FR-mediated uptake.

Based on our previous reactions for Pc-(L-CA4)$_2$, the synthetic scheme was developed using reactions such as esterification, yne-amine, nucleophilic substitution, click, and the amidation reaction, to make the process easily adaptable to other alcohol-containing drugs (Scheme 1). A nucleophilic substitution reaction of a silicon phthalocyanine dichloride yielded compound **6**. Intermediate **7** was synthesized through click (yne-amine) reaction of compounds **6** and combretastatin A-4 propiolate (CA4—CO—C≡C—H) at a 1 to 1 molar ratio for the monofunctionalization. Prodrug **1** was synthesized by the amidation of FA anhydride intermediate generated in situ and compound **7**. Compound **7** was esterified at room temperature with 5-hexynoic acid to yield compound **8**. Compound **13** was synthesized through multiple steps (Scheme S1 in SI). A click reaction between compounds **8** and **13** using PMDETA and CuBr at 37 °C yielded prodrug **2**. Compound **9** was synthesized by the amidation of compound **7**

dx.doi.org/10.1021/bc500376j | Bioconjugate Chem. 2014, 25, 2175−2188

and diglycolic anhydride at room temperature. Amidation of compound **9** with **17** (Scheme S2 in SI) or **NH_2-$PEG_{\sim 45}$-FA** (purchased from Nanocs, Inc.) yielded prodrugs **3** and **4**, respectively. Monoprotection of diamine (compound **14**, Scheme S2 in SI) using di-*tert*-butyldicarbonate by refluxing under basic conditions gave compound **15**. Amidation and deprotection of **15** gave **17** (Scheme S2 in SI). Finally, prodrug **5** was synthesized by the amidation of compounds **9** and **15**. All steps were straightforward, versatile, and high yielding, with yields above 50%. We relied primarily on the ESI method to determine the masses of our compounds containing amino-acrylate linker, since the linker was highly sensitive to light.

Photophysical Studies. Electronic absorption properties of the prodrugs measured in DMF and partition coefficients between *n*-octanol and pH 7.4 buffer (log $D_{7.4}$) are listed in Table 1. The UV−vis absorption spectra of all prodrugs (Figure S1 in SI) showed typical absorptions of silicon phthalocyanine with a sharp and intense Q-band at 673−675 nm, which follows the Lambert−Beer law (Figure S1 in SI), indicating that the prodrugs remained nonaggregated in DMF. From the Q-band absorptions, we could further deduce that there was no change in electronic absorption properties of the conjugates by linking the silicon-(IV) phthalocyanine core to the ligands, two bulky axial side-chains.[53]

The partition coefficients of the conjugates are expressed as Log $D_{7.4}$ values. Overall, prodrugs **1** and **2** without or with a shorter PEG spacer had higher log $D_{7.4}$ values than prodrugs **3** and **4** with longer PEG spacers. That is, prodrugs **1** and **2** were more lipophilic, while prodrugs **3** and **4** were more hydrophilic. It was evident that the PEG length impacted the solubility of the prodrugs, at least among these analogs. As expected from the structures, **5** had higher log $D_{7.4}$ (less hydrophilic) than **3** (0.65 vs −0.05), due to the more hydrophilic FA compared to lipophilic *tert*-butoxycarbonyl (boc) group.

Cellular Uptake to Cultured FR-Positive Colon 26 Cells. In order to establish structure-FR-mediated uptake relationships, the time-dependent uptake of prodrugs **1**−**5** was determined using FR-positive colon 26 cells.[54] First, a clear relationship between partition coefficient (log $D_{7.4}$ value) and cellular uptake was observed; that is, lower log $D_{7.4}$ corresponded with higher uptake (Figure 4A). Hydrophilic prodrugs **3** and **4** had much higher uptake throughout the observation time period up to 24 h than the more lipophilic FA-conjugated prodrugs **1** and **2** ($p < 0.001$). During the experimental procedures, it was observed that hydrophilic prodrugs **3** and **4** aggregated less in culture media than did hydrophobic prodrugs **1** and **2**. In addition, the FA group might facilitate the uptake of the prodrugs **3** and **4** via FR-mediated uptake mechanisms. Compared to prodrug **5**, the non-FA conjugated version of prodrug **3**, prodrug **3** had significantly higher cellular uptake over a period of 3−24 h ($p < 0.001$). These results support our hypothesis that FR facilitates higher uptake of less aggregating, hydrophilic prodrugs **3** and **4**.

Impact of Excess Free FA in Culture Medium on the Cellular Uptake of Prodrug. The dependence of uptake of prodrugs **3** and **4** on FR was further evaluated by performing a competitive uptake assay in the presence of excess free FA (1 mM, 100-fold excess) in the culture medium. The excess FA significantly reduced the uptake of prodrugs **3** and **4** ($p < 0.001$) at 24 h by 80% and 73%, respectively, while the cellular uptake of non-FA conjugated prodrug **5** was not significantly influenced ($p > 0.6$, Figure 4B). These results suggest (1) that the main uptake pathway for prodrugs **3** and **4** into the FR+ cells was FR-mediated endocytosis, consistent with the above uptake data and (2) that the uptake of non-FA prodrug **5** was not mediated by FR.

Phototoxicity and Dark Toxicity. To find the effects of the cellular uptake on the prodrugs' cell kill, we determined the phototoxicity of these prodrugs (Figure 5). Briefly, colon 26

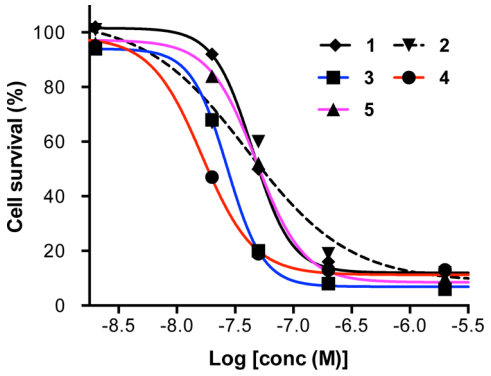

Figure 5. Phototoxicity of prodrugs **1**−**5** against colon 26 cells. Cells were incubated with the prodrugs for 7 h, washed 3 times with PBS, and then illuminated with 690 nm at 5.6 mW/cm^2 for 30 min (10 J/cm^2). Cell viability was determined with MTT assay 72 h after the illumination, and expressed as mean percentage ± SD ($n = 3$) with respect to untreated control cells. (N.B. SD is not presented here.)

cells were incubated with the prodrugs at variable concentrations for 7 h. Cells were then washed three times, and exposed to laser light (690 nm) at 5.6 mW/cm^2 for 30 min (10 J/cm^2). Based on our previous study, such a condition of illumination could be sufficient enough to cleave most of linkers in the prodrugs.[21] Higher cellular uptake was associated with more cell death (**4** and **3** > **2** and **1**). FA-conjugated prodrug was more potent than non-FA conjugated analogue (**3** > **5**). IC_{50} values were 1.65, 2.71, 4.03, 4.47, and 4.85 × 10^{-8} M for **4**, **3**, **2**, **1**, and **5**, respectively. From the phototoxicity results, we concluded that increasing the PEG length not only increases the solubility (hydrophilicity) of the prodrug, but also increases both uptake and cell death. All conjugates were noncytotoxic (>70% cell survival) in the dark at <2 μM (Figure S3 in SI).

In Vivo Optical Imaging. After in vitro cellular uptake experiments, we continued with the preclinical optical imaging study. Because these prodrugs have the same fluorescence photosensitizer, Pc, we expected that all prodrugs could be imaged using a preclinical optical imaging system (IVIS imaging system), and that FR-mediated uptake in tumors could be readily visualized. Each prodrug (2 μmol/kg in 200 μL) was injected IV into Balb/c mice bearing SC colon 26 tumors on the lower back neck region (3 mice/group). Figure 6A shows images of the mice at various time points postinjection.

Interestingly, the mice injected with prodrug **4** showed specific intense emission spots around tumors (Figure 6A, iv) at 7 h. The mice injected with prodrug **1** did not display such bright tumor spots, but showed the overall minimal emission from the entire back. Images from mice injected with prodrugs **2** and **3** showed moderate emission. Consistent with the in vitro uptake results, there was a relationship between the length of the PEG spacer and tumor localization. Prodrugs with longer PEG spacers were taken up more in tumors, presumably via FR-mediated uptake. It seemed that the lipophilic prodrug **1** was not distributed to the skin or tumors, or the emission of two prodrugs was minimal, possibly due to aggregation

dx.doi.org/10.1021/bc500376j | *Bioconjugate Chem.* 2014, 25, 2175−2188

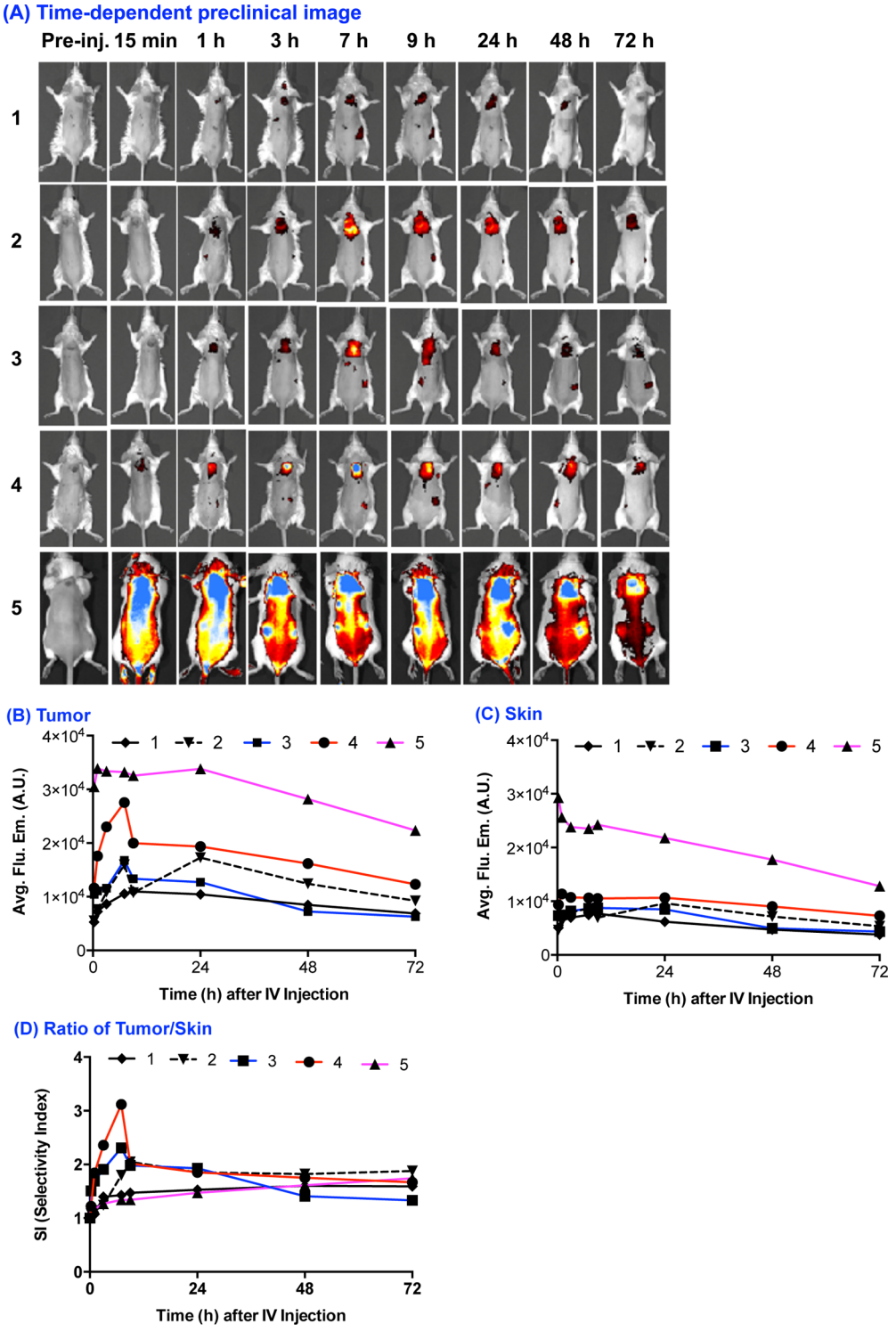

Figure 6. (A) Time-dependent preclinical fluorescence images of prodrugs **1**−**5**. Images of Balb/c mice (n = 2 for prodrugs **1**, **2**, **5**; n = 3 for prodrugs **3**, **4**) bearing SC colon 26 tumors were taken before drug administration and at 0.25, 1, 3, 7, 9, 24, 48, and 72 h post IV injection of the prodrugs (2 μmol/kg). Images were scaled to the same maximum (30 000 A.U.) and minimum values (11 000 A.U.). (B) Average photon emission from tumor of mice IV injected with prodrugs. (C) Average photon emission from selected skin area of mice IV injected with prodrugs. (D) Selectivity index (tumor/skin ratio of emission). Counts are presented as an average of two or three mice in each group. (N.B. SD are not represented here.)

observed during the experimental procedures. The mice injected with non-FA-conjugated prodrug **5** showed a somewhat distinct image pattern: bright but broader spots around tumors, higher emission throughout the entire back, and two bright spots that were presumed to be the kidneys. The distribution of prodrug **5** seemed to be higher, but less specific to tumors, than the distribution of prodrug **4**, suggesting that the localization of **5** might not be primarily mediated by FR.

To estimate the concentrations of the prodrugs in tumors and skin, average emission intensities were calculated from

dx.doi.org/10.1021/bc500376j | Bioconjugate Chem. 2014, 25, 2175−2188

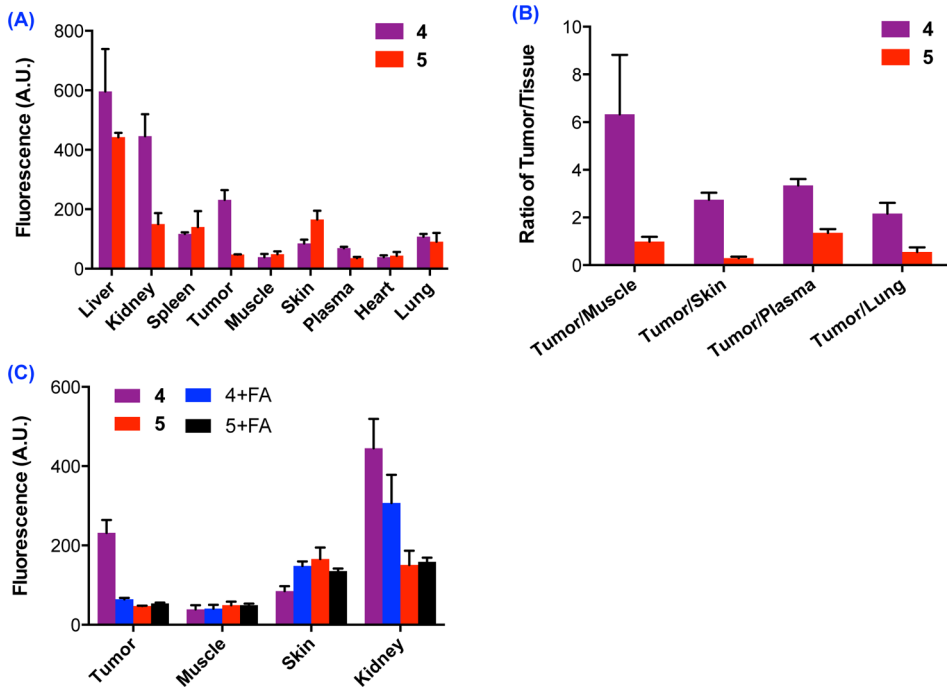

Figure 7. Tissue distribution of the IV injected prodrugs **4** and **5** in mice bearing SC colon 26 tumors. (A) Fluorescence emission from homogenized tissues. (B) Ratios of fluorescence emission of tumor to fluorescence emission of tissues. (C) Fluorescence emission from homogenized tissues without and with preadministration of excess FA (100×). Data are averages and SD of samples from three mice.

these images (Figure 6A,B). The ratios of tumor to skin (Figure 6C) were plotted. As shown, prodrug **4** demonstrated higher (27 023 A.U.) and more selective tumor uptake (tumor/skin ratio = 3:1) at 7 h than did the other prodrugs. Prodrug **1** showed lower emission (~10 559 A.U.). Prodrugs **2** and **3** showed some localization to tumors (tumor/skin ratios = 2:1 and 2:1). Prodrug **5** showed the highest uptake in both tumor (32 175 A.U.) and skin (22 585 A.U.), compared with the other prodrugs, but uptake was not selective (tumor/skin ratio = 1.4:1).

Tissue Distribution of Prodrugs 4 and 5. Because the preclinical imaging data show prodrug distribution more accurately in superficial areas such as tumor surface and skin, a conventional biodistribution study was performed to understand the tissue distribution of two prodrugs, **4** (the best FA-conjugated prodrug) and **5** (non-FA-conjugated, control prodrug), in detail. Various tissue samples were collected 7 h after IV administration of these prodrugs (3 mice per group). Collected tissue samples (150 mg) were dissolved in 1 mL DMSO, homogenized, and then centrifuged. Fluorescence of the supernatant was read (emission at 605 nm and absorption 640−750 nm).

Consistent with the preclinical optical imaging data, the fluorescence emission of tumors (232 A.U.) from the mice injected with prodrug **4** was significantly higher than emission from skin (85 A.U.) and muscle (39 A.U., $p < 0.01$, Figure 7A). The ratios of tumor/muscle and tumor/skin were 6:1 and 3:1 (Figure 7B). Fluorescence emission of skin (166 A.U.) from the mice injected with prodrug **5** was higher than that (85 A.U.) from the mice injected with prodrug **4** ($p < 0.01$). However, low emission of tumors (47 A.U.) was observed from mice treated with prodrug **5**, which contrasts with the preclinical optical imaging data showing high emission from broad tumor areas (Figure 6A). We assume that the higher emission of tumor areas of the mice injected with **5** could be due to the higher concentration of **5** in skin on the tops of the tumors. This finding *reminds us that the preclinical optical imaging data should be assessed with care and with the help of complementary methods.* Non-FA-conjugated prodrug **5** did not show such selective uptake in tumors: the ratios of tumor/muscle and tumor/skin were 1:1 and 1:3. Overall, the tissue distribution study confirmed the higher uptake of FA-conjugated prodrug **4** in tumors over other skin and muscle, probably due to FR-mediated uptake in tumors.

To see the impact of excess of free FA in mice to the uptake of prodrugs **4** and **5**, tissue uptake of prodrugs **4** and **5** was determined after pre-IP-injected excess of FA (100×) (Figure 7C). We expected a significant decrease of prodrug **4** uptake in FR-positive tissues (e.g., FR-positive colon 26 tumor and FR-rich kidney) because free FA could interfere with the FR-mediated uptake. Indeed, the free FA reduced the tumor uptake of prodrug **4** (72%) as well as the FR-rich kidney uptake (31%). On the other hand, the free FA had a minor impact on the tumor and kidney uptake of non-FA-conjugated prodrug **5**, with 14% and 5% increase in tumor and kidney uptake, respectively. These results strongly support our analysis that FR-mediated uptake has a major role in the uptake of FA-conjugated prodrug **4** into FR-positive colon 26 tumor.

Selective and Effective Tumor Damage by Treatment with Prodrug 4. Enhanced delivery of FA-conjugated prodrug **4** to FR-positive colon 26 tumors led us to evaluate selective damage to tumors over skin damage in the illuminated areas. Balb/c mice (3 mice per group) with SC colon 26 tumors were treated with prodrugs **4** and **5** (as a positive comparison). When tumors reached 4−6 mm diameter, the mice were IV injected with 2 μmol/kg of prodrug **4** or **5** in 200 μL 5% Cremophor EL in PBS. Then, 7 h post-injection, we illuminated a 12 mm area centered on the tumor with a 690 nm laser (100 mW/cm^2 for 30 min, 180 J/cm^2; Figure 8A).

dx.doi.org/10.1021/bc500376j | *Bioconjugate Chem.* 2014, 25, 2175−2188

The treatment conditions were based on our previous studies.[20] The mice were imaged and volumes of tumors were measured.

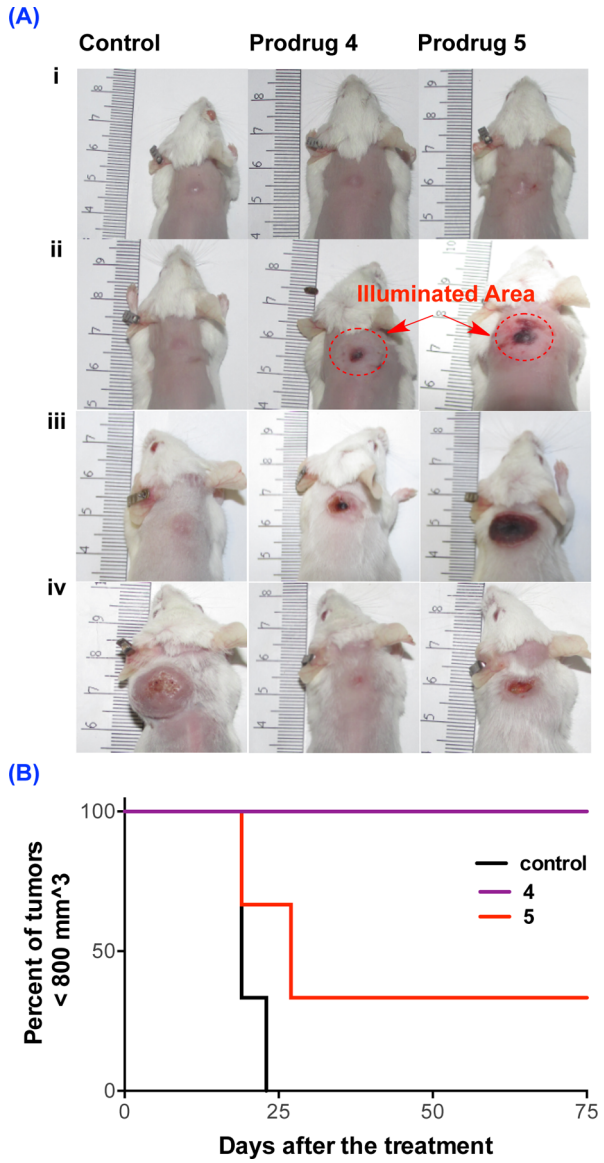

Figure 8. (A) Photographic images of mice (3 mice per group) treated with prodrug (none, **4**, or **5** at 2 μmol/kg) with illumination (690 nm laser, 12 mm diameter circular beam, 100 mW/cm^2, 30 min) 7 h post IV administration of the prodrug: (i) day 0 before illumination, (ii) day 1, (iii) day 6, and (iv) day 15 post-illumination. (B) Kaplan–Meier plot of response to treatment.

There was an apparent difference between mice treated with prodrug **4** and mice treated with prodrug **5**, in terms of the damage to the illuminated area (Figure 8A). Damage to the surrounding skin in the illuminated area was less in mice treated with prodrug **4** (days 1 and 6), due to the higher tumor/skin ratio. In mice treated with prodrug **5**, the surrounding skin showed more severe damage and slower healing (day 15), possibly due to the higher concentration of **5** in the skin (tumor/skin ratio = 1:3).

In the antitumor efficacy study (Figure 8B), all three mice treated with prodrug **4** were tumor-free until day 75. The tumors seemed to be removed. Two of three mice treated with prodrug **5** had large tumors (>800 mm^3) on days 19 and 23. The outstanding antitumor effect of **4** should be due to the high concentration of the prodrug **4** in tumor. The FA-targeting was effective not only for selective delivery to tumors, sparing the skin in the illuminated area, but also for enhanced delivery to tumors, improving the antitumor efficacy. No significant body weight loss was observed in any group (Figure S2 in SI), indicating no acute toxicity during the treatment period.

CONCLUSIONS

Targeted multifunctional prodrugs were designed to achieve selective and enhanced delivery of SO-cleavable prodrugs to tumors. The prodrugs express the combined effects of PDT and local chemotherapy. Nontargeted prodrug **5** and FA-conjugated prodrugs **1**–**4**, with varying lengths of a PEG spacer, were prepared via straightforward and versatile synthetic routes. From the above studies, we draw the following conclusions.

The length of the PEG spacer made a significant impact on the partition coefficients (log $D_{7.4}$) between *n*-octanol and pH 7.4 buffer of these prodrugs. Prodrugs **3** and **4** had longer PEG units and lower log $D_{7.4}$ than did prodrugs **1** and **2** with shorter PEG spacers. Cellular uptake of prodrug **3** and **4** to cultured FR-positive colon 26 cells was also significantly higher than that of prodrugs **1**, **2**, and **5**. The enhanced uptake of prodrugs **3** and **4** seemed to be mediated by FR. The enhanced uptake also resulted in higher cell kill. Prodrugs **3** and **4** showed more specific delivery to tumors compared with prodrugs **1**, **2**, and **5**. Prodrug **4** had the longest PEG spacer and was the best at delivering drug to tumors. Compared with non-FA-targeted prodrug **5**, prodrug **4** showed higher and more selective uptake to tumors, presumably due to FR-mediated uptake. This resulted in selective and effective tumor damage, sparing the skin in the illuminated area. In clinical settings, a broad area around a tumor must be illuminated in order to have a margin for complete ablation of tumor. Therefore, sparing the normal tissues surrounding tumors is crucial, especially when the tumors reside in critical organs. We proved that FA-targeting of SO-cleavable prodrug could be effective in achieving that goal.

We envision that this targeted prodrug concept can be adoptable to many other applications because the prodrug system is simple but highly flexible. All three components, PS, Drug, and targeting groups can be easily substituted with others as needed for specific disease types. Quantitative understanding of both cellular and pharmacological mechanisms of prodrugs, in particular, with temporal and spatial resolution, will provide an opportunity for achieving more in synergistic effects of PDT and site-specific chemotherapy. Tunability of two therapeutic effects (PDT vs drug effects) will also provide new opportunities beyond the oncological applications. These are the basis of our current studies.

EXPERIMENTAL PROCEDURES

Materials and Methods. All commercially available chemicals were of analytical grade and were used without further purification. Solvents and reagents were obtained from Sigma-Aldrich or Fisher Scientific. PEG-diamine (compound **14**, Scheme S1 in SI) was purchased from Polypure AS, Gaustadaleen 21, N-0349. Oslo, Norway (Cat #: 12112–1892, MW = 897), while H_2N-PEG$_{\sim 45}$-FA was obtained from Nanocs Technology, Inc. (Cat #: PG2-AMFA-2k, MW = ~2000). Analytical thin layer chromatography (TLC) was performed on aluminum-backed 5–17 μm silica gel plates with fluorescent indicators from Sigma-Aldrich (Cat #Z193291–1PAK). All

dx.doi.org/10.1021/bc500376j | *Bioconjugate Chem.* 2014, 25, 2175–2188

chromatography was performed using 32−63 μm silica gel from Sorbent Technologies (Cat #02826−26). Preparative TLC was performed on glass-backed plates precoated with silica with UV254 prep-scored 20 × 20 μm from Analtech Inc. (Catalog #02003). All dialysis was performed using 7 Spectra/Por dialysis membrane (MWCO: 1000 Da) from Spectrum Laboratories, Inc. Gel filtration chromatography were performed using either Sephadex LH-20 (Cat #17−0090−10) or Sephadex G-15 obtained from GE Healthcare Bio-Science AB. Deuterated solvents (NMR solvents with residual solvent signals as internal standards) were purchased from Cambridge Isotopes Laboratories or Sigma-Aldrich. NMR spectra were recorded at 25 °C with a 300 MHz spectrometer (Varian Mercury). Representative NMR spectra are found in SI. High-resolution mass spectra (HRMS) were collected using an Agilent 6538 UHD Accurate Mass QTOF (Santa Clara, CA) equipped with an electrospray ionization source at the Mass Spectrometry Facility at the University of Oklahoma. Low-resolution mass spectra (LRMS) were acquired using Ion Trap Bruker Daltonics HCT Ultra PTM Discovery system with ESI source at the CORE Facility of OUHSC. Representative MS spectra are found in the SI.

Purity was evaluated by analytical HPLC using a waters HPLC system (waters-501 solvent delivery system, SPD-10AV shimadzu UV−vis detector, a U6K-03696 autoinjector), coupled to a chromatography data system N2000. HPLC chromatograms of prodrugs **1**, **2**, **3**, and **5** are found in SI. HPLC chromatogram of prodrug **4** could not be made because it was not a single compound. Thus, we used ^{1}H NMR spectra to determine its identity and purity (SI Figures S30−32). Mobile phase was pumped at a flow rate of 0.6 mL/min. A μBondapak C_{18} (5 μM) column (250 × 4.6 mm I.D. 12109949TS) was used; this was preceded by a guard column containing C_{18}/Corasil Bondpak (particle size 37−50 μM). Detection was effected at 254 and 350 nm, and an isocratic condition was used.

The optical images of live mice (Figure 6A and SI Figure S37) were obtained using the IVIS spectrum (PerkinElmer, Inc.) with Live Image software. Weighing of compounds and acquisition of in vivo images were done under minimal light conditions. Female Balb/c mice were purchased from Charles River Laboratories, Inc. through NCI (Frederick, MD). Mice were housed and handled in the animal facility of the College of Pharmacy or Rodent Barrier Facility in the Biomedical Research Center-West at the University of Oklahoma Health Sciences Center (OUHSC), Oklahoma City, OK. All animal experiments were approved by IACUC, OUHSC. This mouse tumor model (colon 26 cells on Balb/c mice) was chosen, not because we want to demonstrate the efficacy of the prodrugs to colon tumor, but because this tumor model has FR, has an intact immune system, and has been commonly used in PDT studies.

Compounds **10** and **14** were purchased. Compounds **CA4** propiolate,[19] **6** (Scheme 1),[20] **11** (Scheme S1 in SI),[55] **12** (Scheme S1 in SI),[55] and **13** (Scheme S1)[56] were prepared based on methods in the previous reports.

Compound 7. Compound **6** (0.38 g, 0.47 mmol) was added to a 150 mL dry THF solution in a round-bottom flask. The solution was purged and maintained for 10 min in N_2 atmosphere. CA4 propiolate (0.17 g, 0.47 mmol) dissolved in 30 mL dry THF was then added dropwise into a vigorously stirred solution of **6** over 1.5 h, and then allowed to stir for an additional 15 min. The reaction mixture was evaporated under reduced pressure and the crude product was purified using either the preparative TLC or a short column chromatography first, using the solvent system ethyl acetate/methanol (4:1 v/v) to remove the disubstituted product, followed by DCM/MeOH/NH_4OH (79:17:4 v/v/v) to afford the target compound 7 as a blue solid (320 mg, 58%). ^{1}H NMR (300 MHz, CD_2Cl_2-d_2): 9.67 (br s, m, 8H), 8.38 (br s, 8H), 7.19 (d, J = 11.9 Hz, 1H), 7.00 (m, 2H), 6.85 (d, J = 11.9 Hz, 1H), 6.52 (s, 2H), 6.46 (m, 2H), 4.35 (d, J = 12.99 Hz, 1H) 3.76 (s, 3H, OMe), 3.70 (s, 3H, OMe), 3.65 (s, 6H, OMe), 2,19 (br s, 8H), 1.65 (br s, 1H, NH), 0.29 (br s, 8H), −0.37 (m, 4H), −1.94 (m, 4H). HRMS (ESI): calcd. for $C_{65}H_{63}N_{12}O_8Si$ $[M + H]^+$: 1167.4661 and $C_{65}H_{61}N_{12}O_8SiNa$ $[M + Na]^+$: 1189.4481, found: 1167.4665 and 1189.4479.

Compound 8. 5-Hexynoic acid (0.019 g, 0.17 mmol), *N,N*-diisopropylethylamine (DIPEA) (56.6 μL, 0.044 g, 0.34 mmol), and *O*-(benzotriazol-yl)-*N,N,N′,N′*-tetramethyluronium hexafluorophosphate (HBTU, 0.065 g, 0.17 mmol) were added to a 5 mL dry DCM stirring solution of compound 7 (0.10 g, 0.085 mmol). The reaction mixture was left for 2 h at room temperature and monitored using TLC. At the end of the reaction, the reaction mixture was diluted with 60 mL of DCM and washed with 200 mL water three times. The organic filtrate was then dried using anhydrous sodium sulfate (Na_2SO_4) and evaporated to dryness in vacuo. The crude was redissolved in minimum DCM, and then recrystallized using a mixture of cold hexane/Et_2O. The solid residue was washed several times with diethyl ether to afford a deep blue solid product (87 mg, 81%). ^{1}H NMR (300 MHz, CD_2Cl_2-d_2): 9.67 (br s, m, 8H), 8.38 (br s, 8H), 7.19 (d, J = 11.9 Hz, 1H), 7.00 (m, 2H), 6.85 (d, J = 11.9 Hz, 1H), 6.52 (s, 2H), 6.46 (m, 2H), 4.35 (d, J = 12.99 Hz, 1H) 3.76 (s, 3H, OMe), 3.70 (s, 3H, OMe), 3.65 (s, 6H, OMe), 2.51 (s, 1H) 2,19 (br s, 8H), 1.95(m, 2H), 1.56 (m, 4H), 0.29 (br s, 8H), −0.37 (m, 4H), −1.94 (m, 4H). ^{13}C NMR (75 MHz, CD_2Cl_2-d_2): 168.72, 167.32, 153.12, 152.24, 151.19, 149.26, 140.33, 137.35, 135.59, 132.43, 131.39, 129.98, 129.11, 128.76, 126.65, 123.50, 112.11, 105.97, 81.96, 70.74, 60.40, 56.37, 55.83, 42.87, 41.41, 31.31, 22.54, 13.78. HRMS (ESI): calcd for $C_{71}H_{69}N_{12}O_9Si$ $[M + H]^+$: 1261.5090 and $C_{71}H_{68}N_{12}O_9SiNa$ $[M + Na]^+$: 1283.4899, found: 1261.5077 and 1283.4891.

Compound 9. Compound 7 (0.084 g, 0.072 mmol) and diglycolic anhydride (0.0084 g, 0.072 mmol) were added to 6 mL anhydrous DMF in 10 mL round-bottom flask equipped with a magnetic stir bar at room temperature, and allowed it to run for 36 h. The reaction mixture was poured dropwise into cold diethyl ether (Et_2O). The blue precipitate was filtered using a sintered glass funnel. This was further washed with more diethyl ether solvent to obtain a blue solid (64 mg, 69%). ^{1}H NMR (300 MHz, CD_2Cl_2): 9.67 (br s, m, 8H), 8.38 (br s, 8H), 7.19 (d, J = 11.9 Hz, 1H), 7.00 (m, 2H), 6.85 (d, J = 11.9 Hz, 1H), 6.52 (s, 2H), 6.46 (m, 2H), 4.35 (d, J = 12.99 Hz, 1H), 3.98 (s, 2H), 3.91 (s, 2H) 3.76 (s, 3H, OMe), 3.70 (s, 3H, OMe), 3.65 (s, 6H, OMe), 2,19 (br s, 8H), 1.65, 0.29 (br s, 8H), −0.37 (m, 4H), −1.94 (m, 4H). ^{13}C NMR (75 MHz, CD_2Cl_2): 169.74, 167.47, 152.98, 152.29, 151.20, 149.41, 140.24, 135.88, 132.39, 131.30, 129.82, 129.12, 128.42, 126.56, 123.91, 123.60, 111.78, 105.95, 83.86, 81.68, 68.39, 60.38, 55.80, 51.21, 44.06, 40.25, 31.17, 23.79, 17.72. HRMS (ESI): calcd for $C_{69}H_{67}N_{12}O_{12}Si$ $[M + H]^+$: 1283.4771, found: m/z 1283.4781.

Compound 15 (Scheme S2 in SI). A stirring solution of a commercially available diamine (compound **14**; 500 mg, 0.56

mmol) in anhydrous MeOH (9.31 mL) was treated with Boc_2O (123 mg, 0.56 mmol) and triethylamine (TEA) (178 μL, 1.67 mmol).[57] The reaction mixture was left to reflux for 24 h. The solvent was removed under reduced pressure and the resulting yellow oil was purified by silica gel chromatography using DCM/MeOH/NH_4OH (79:17:4% v/v/v) as the eluent to give **15** as a colorless/white solid after freezing (400 mg, 72%). ^1H NMR (300 MHz, D_2O-d_2): 3.64 (br s, $-CH_2-$ of PEG), 3.20 (m, 4H), 3.00 (m, 4H), 1.43 (s, 9H, *t*-butyl group). LRMS (ESI): calcd for $C_{45}H_{93}N_2O_{21}$ $[M + H]^+$: 997.63, found: *m*/*z* 997.70.

Compound 16 (Scheme S2 in SI). To a stirring solution of FA (0.083 g, 0.19 mmol) in anhydrous DMF/pyridine (5:1 v/v) solution, DCC (0.23 g, 1.13 mmol) was added in one portion.[57] The reaction mixture was kept in an ultrasound bath in the dark for 30 min. Then, the resulting suspension was quickly filtered over a sintered funnel and the precipitate was washed with a minimum amount of DMF/pyridine solution. Boc-PEG amine (**15**; 180 mg, 0.19 mmol) was then added to the filtrate and allowed to stir in the dark for 36 h. The reaction mixture was then poured dropwise into a stirred solution of cold Et_2O/acetone (4:1 v/v) to afford a yellow precipitate that was collected on a sintered glass funnel. After washing several times with cold acetone and Et_2O, the material was dried to give a deep yellow solid product. This was further purified by passing over Sephadex G-15, using deionized water as a solvent to remove any unreacted folic acid (196 mg, 73%). ^1H NMR (300 MHz, D_2O-d_2): 8.60 (s, 1H), 7.52 (br s, 2H), 6.62 (br s, 2H), 3.52 (br s, $-CH_2-$ of PEG block), 1.27 (s, 9H, *t*-butyl group). LRMS (ESI): calcd. for $C_{64}H_{110}N_9O_{26}$ $[M + H]^+$: 1420.76, found: *m*/*z* 1420.70.

Boc-deprotection on compound **16** was accomplished using TFA at room temperature. The deprotected product (**17**) was used for the next step without further purification, after drying under high vacuum.[57]

Prodrug 1. Prodrug **1** was synthesized from FA following a modified procedure from the literature.[57] To a stirring solution of FA (0.015 g, 0.034 mmol) in anhydrous DMF/pyridine (5:1 v/v) solution, DCC (0.043 g, 0.21 mmol) was added in one portion (Figure S1 in SI). The reaction mixture was kept in an ultrasound bath in the dark for 30 min. Then, the resulting suspension was quickly filtered over a sintered funnel and the precipitate was washed with minimum amount of DMF/pyridine solution. A solution of **7** (0.040 g, 0.034 mmol) was added into the filtrate. The resulting mixture was further stirred at room temperature in the dark for 24 h. The crude reaction mixture was then purified by passing through a gel permeation G-15 Sephadex column, using DMF as the eluent to separate the product from the unreacted folic acid starting material. The top stop was then collected and poured dropwise into a stirred solution of cold Et_2O/acetone (4:1 v/v) to afford a green precipitate that was collected over a sintered glass funnel. An alternative method was simply to precipitate it in cold Et_2O/acetone (4:1 v/v), followed by dialysis in DMF with cellulose membrane of MWCO of 1000 Da for 48 h. After washing several times with cold acetone and Et_2O, the material was dried to give a deep blue solid product (34 mg, 62%) with more than 96% purity (Figure S22 in SI). ^1H NMR (300 MHz, DMSO-d_6): 9.67 (br s, 8H), 8.65 (s, 1H), 8.49 (m, 8H), 7.64 (d, *J* = 7.75 Hz, 2H), 7.11−6.90 (m, 5H), 6.67 (d, *J* = 8.0 Hz, 2H), 6.55 (br s, 2H), 6.48 (m, 2H), 4.49 (br s, 2H), 4.30 (d, *J* = 11.43 Hz), 4.17 (m, 1H), 3.71 (s, 3H, OCH_3), 3.61 (s, 9H, 3 × OCH_3,), 2.35 (m, 2H), 2.20 (br s, 8H), 1.21 (br s 2H), 0.22−0.12 (m, 8H), −0.7 (m, 4H). ^{13}C NMR (75 MHz, DMSO-d_6): 166.64, 152.98, 152.98, 151.33, 149.25, 140.37, 135.42, 132.57, 132.41, 129.02, 124.03, 112.86, 106.39, 60.48, 56.11, 56.06, 31.16. HRMS (ESI): calcd. for $C_{84}H_{79}N_{19}O_{13}Si$ $[M + H]^+$: 1590.5952, found: 1590.5930.

Prodrug 2. Compounds **13** (0.020 g, 0.033 mmol) and **8** (0.042 g, 0.033 mmol) were dissolved in 1.5 mL anhydrous DMF. After purging with nitrogen gas at room temperature, *N,N,N′,N″,N″*-pentamethyldiethylenetriamine (PMDETA; 0.0058 g, 0.033 mmol) and CuBr (0.0048g, 0.033 mmol) were added and the solution was stirred at 37 °C for 48 h. Opening it to air stopped the reaction. The mixture was then diluted with DMF. It was washed with water to eliminate copper. The crude was extensively dialyzed against DMSO for 72 h (cutoff MW 1000) and then precipitated using cold Et_2O/acetone mixture (4:1 v/v) to afford **2** as green precipitate (37 mg, 60%). HPLC chromatogram indicated a purity of more than 97% (Figure S26 in SI). ^1H NMR (300 MHz, DMSO-d_6): 9.67 (br s, m, 8H), 8.38 (br s, 8H), 7.69 (br s, 2 H), 7.19 (d, *J* = 11.9 Hz, 1H), 7.00 (m, 2H), 6.85 (d, *J* = 11.9 Hz, 1H), 6.52 (s, 2H), 6.46 (m, 2H), 4.35 (d, *J* = 12.99 Hz, 1H), (4.13, s, 2H), 3.76 (s, 3H, OMe), 3.70 (s, 3H, OMe), 3.65 (s, 6H, OMe), 2.19−2.33 (m, 8H), 1.95 (m, 2H), 1.56 (m, 4H), 0.29 (br s, 8H), −0.37 (m, 4H), −1.94 (m, 4H). ^{13}C NMR (75 MHz, DMSO-d_6): 152.98, 152.50, 151.12, 149.26, 140.36, 140.16, 137.15, 135.40, 132.09, 130.05, 129.66, 129.41, 128.99, 124.06, 123.20, 60.71, 60.52, 59.70, 55.57, 47.70, 35.92, 33.78, 33.23, 31.16, 25.77, 24.54. HRMS-ESI: Calcd for $[C_{96}H_{99}N_{23}O_{16}SiNa_2]^{+2}$ $[M+2Na]^{+2}$: 951.8602, found: 951.9423.

Prodrug 3. The procedure for this synthesis was similar to that of prodrug **4**. Briefly, compound **17** (0.082 g, 0.062 mmol), compound **9** (0.080 g, 0.062 mmol), HBTU (0.026 g, 0.069 mmol), and DIPEA (22.80 μL, 0.14 mmol) in 4 mL anhydrous DMF afforded a dark green solid product after similar purification process (101 mg, 63%) with >87% purity (Figure S29 in SI). ^1H NMR (300 MHz, CD_2Cl_2-d_2): 9.67 (m, 8H), 8.40 (m, 8H), 7.69 (m, 1H), 7.41 (m, 2H), 7.10 d, *J* = 11.9 Hz, 1H), 7.00 (m, 2H), 6.85 (m, 2H), 6.52 (br s, 2H), 4.35 (d, *J* = 12.99 Hz, 1H), 3.85 (br s, 2H), 3.78 (s, 4H), 3.73 (s, 3H, OMe), 3.68 (s, 9H, 3 × OMe), 3.58 (br s, complex), 2.21 (m, 8H), 1.67 (br s, 9H), 0.31 (m, 8H), −0.58 (m, 4H, b), −1.90 (br s, 4H). HRMS (ESI): *m*/*z* 2584.1546 calcd for $[C_{128}H_{169}N_{21}O_{35}Si]^{+2}$ $[M+4H]^{+2}$: 1294.5947, found: 1294.6811.

Prodrug 4. Commercially available $NH_2-PEG_{\sim 45}-FA$ (compound **10**; 0.078 g, 0.033 mmol), compound **9** (0.044 g, 0.034 mmol), DIPEA (0.099 mmol), and HBTU (0.019 g, 0.050 mmol) were added to a 4 mL anhydrous DMF in a 10 mL round-bottom flask equipped with a magnetic stir bar and allowed it to stir for 3 h at room temperature. The crude reaction mixture was passed through a G-15 Sephadex column using DMF as the eluent. With the molecular weight of the final product greater than 1500 g/mol, the products passed through the void volume and were collected as the fast moving spot from the solvent front. The product was dialyzed (MWCO of 1000 Da) for 48 h against DMF and, subsequently, against DCM for 12 h to eliminate the DMF. The product in DCM was concentrated in vacuo and precipitated into a sticky dark green solid product using cold Et_2O (71 mg, ∼58%; SI Figure S31 for stacked ^1H NMR of $NH_2-PEG_{\sim 45}-FA$ and **4**). ^1H NMR (300 MHz, DMSO-d_6): 9.67 (m, 8H), 8.40 (m, 8H), 7.96 (br s, NH), 7.69 (m, 1H), 7.41 (m, 2H), 7.10 d, *J* = 11.9

dx.doi.org/10.1021/bc500376j | Bioconjugate Chem. 2014, 25, 2175−2188

Hz, 1H), 7.00 (m, 2H), 6.85 (m, 2H), 6.52 (br s, 4H), 6.46 (m, 1H), 4.35 (d, J = 12.99 Hz, 1H), 4.24 (m, 1H), 3.85 (br s, 2H), 3.78 (s, 4H), 3.73 (s, 3H, OMe), 3.68 (s, 9H, 3 × OMe), 3.58 (br s, complex), 2.91 (s, DMF), 2.82 (s, DMF), 2.21 (m, 8H), 1.67 (br s, H_2O), 0.31 (m, 8H), −0.58 (m, 4H), −1.90 (br s, 4H).

Prodrug 5. This compound was synthesized as a control following the same procedure described for prodrug **4**. Compound **9** (102 mg, 0.080 mmol), compound **15** (75.73 mg, 0.078 mmol), HBTU (33.18 mg, 0.088 mmol), and DIPEA (28 μL, 0.18 mmol) in 4 mL anhydrous DMF gave a green solid (130.0 mg, 74%) with >99% purity (SI Figure S35). ^{1}H NMR (300 MHz, CD_2Cl_2-d_2) [SI Figure S33]: 9.67 (m, 8H), 8.40 (m, 8H), 7.69 (m, 1H), 7.10 (d, J = 11.9 Hz, 1H), 7.00 (m, 2H), 6.85 (m, 1H), 6.52 (br s, 2H), 4.35 (d, J = 12.99 Hz, 1H), 4.24 (m, 1H), 3.85 (br s, 2H), 3.78 (s, 4H), 3.73 (s, 3H, OMe), 3.68 (s, 9H, 3 × OMe), 3.58 (br s, complex), 2.21 (m, 8H), 1.46 (br s, 9H, t-butyl), 0.31 (m, 8H), −0.58 (m, 4H), −1.90 (br s, 4H). HRMS (ESI): m/z = 2261.0779 calcd for $[C_{114}H_{158}N_{14}O_{32}Si]^{+2}$ $[M+2H]^{+2}$: 1131.5468 (81.1%) and 1132.0462 (100%), found: 1131.5644 (81.1%) and 1132.0611 (100%).

Log $D_{7.4}$. n-Octanol/pH 7.4 buffer partition coefficients of all five conjugates were determined by "shake flask" direct measurement.[58] Saturated solutions of conjugates were prepared by adding 10 μL of 4 mM DMSO stock solutions to a mixture of equal volumes of 1 mL n-octanol and a pH 7.4 phosphate buffer. The saturated solutions were vigorously shaken for 30 min using a shaker, and then were allowed to settle for 4 h. Then, 100 μL of each layer was diluted to 1 mL with DMF and the absorbance of the prodrug conjugates in the respective solutions were determined. The partition coefficients were obtained by calculating the ratio of the absorbance of the conjugates in the two layers and the results reported as Log $D_{7.4}$ value. Experiments were performed in triplicate.

General Conditions for Colon 26 Cell Culture. Mouse colon adenocarcinoma (colon 26) cells,[54] which are FR-positive, were used for all biological experiments. All reagents and culture media were obtained from Invitrogen and Sigma-Aldrich. The cells were grown in low glucose Dulbecco's Modified Eagle's Medium (DMEM, 4.0 g/L glucose) supplemented with 10% (v/v) fetal bovine serum, 1% antibiotics (100 units/mL penicillin G, 100 μg/mL streptomycin), and 2 mM L-glutamine. The cells were maintained continuously in culture media and subcultured biweekly to maintain approximately 80−90% confluence. A BioTek plate reader (Synergy 2) was used to read UV/vis absorbance. A Molecular Device fluorescence plate reader (Gemini EM) was used to read the fluorescence. The incubation was at 37 °C under humidified atmosphere of 5% CO_2 using a Sanyo MCO-18AIC-UV incubator. Colon 26 cells were seeded at (2−5) × 10^4 cells/well in 200 μL media in 96-well microplates for 24 h before the experiment, to allow cell attachment.

Cellular Uptake to Cultured Colon 26 Cells. To determine the intracellular accumulations of all prodrugs (**1**−**5**), colon 26 cells[54] were seeded in 96-well plates at 5 × 10^4 cells/well in 200 μL complete medium and were incubated at 37 °C in 5% CO_2 for 24 h. The 4 mM stock solutions of the conjugates in DMSO were diluted to 100 μM with a Cremophor formulation mixture composed of PBS/EtOH/Cremophor (18:1:1 v/v/v), before solutions were added to the wells. The respective diluted solutions were then added to complete medium in each well to achieve a 10 μM final concentration of conjugate per well, and the well plates were incubated at various time points. After every incubation time point, the medium was removed and the cell monolayer was rinsed thrice with cold PBS. We then added 100 μL of DMSO to each well to solubilize the cells for 5 min, after which an additional 100 μL of absolute EtOH was added. The fluorescence from phthalocyanine (Pc) was read using the multiwell plate reader (Molecular Devices, SpectraMax M2 model) set at 605 nm excitation and 640−800 nm emission wavelengths. The intracellular accumulation of the conjugates was expressed in fluorescence units (A.U.).

Dark and Phototoxicity. The cytotoxicity of all five conjugates was determined in colon 26 cells with and without illumination.[54] Briefly, cells were grown in tissue culture flasks (75 cm^2) and maintained under 5% CO_2 atmosphere at 37 °C. DMEM supplemented with 10% bovine growth serum, 1% (v/v) L-glutamine, and 1% antibiotics (100 units/mL penicillin G and 100 μg/mL streptomycin) was used as the growth medium and changed on alternate days. The cells were harvested with a 0.25% w/c trypsin-EDTA solution, once 90% confluence was achieved. Cells were subcultured in 190 μL of the complete medium in 96-well culture plates at a density of (1.0−1.5) × 10^4 cells/well, followed by incubation for 24 h. 10 μL of the respective diluted solutions of the conjugates (previously diluted from the 4 mM stock solution to the appropriate concentrations using complete media) were then added to the complete medium in each well to achieve final concentrations ranging from 0.1 nM to10 μM. The plates were then incubated for 7 h.

Phototoxicity Study. The medium in each well was removed and cell monolayers were washed three times with ice-cold PBS (190 μL) to remove any unbound fluorescence. 190 μL of fresh medium was then added to each well and illuminated the uncovered plate for 30 min using a diode laser (690 nm, 5.6 mW/cm^2) while gently shaking using an orbital shaker (Labline, Barnstead International). The plates were incubated for a further 3 days at 37 °C in 5% CO_2, after which cell viability was determined by MTT. Briefly, a volume of 10 μL of MTT at a concentration of 10 mg/mL was added to 190 μL of complete media in each well. After 4 h of incubation, MTT solutions were removed and formazan crystals formed were dissolved in 200 μL of DMSO while shaking for 10 min. The absorbance was measured at 570 nm with background subtraction at 650 nm. The cell viability (%) was then quantified by measuring the absorbance of the treated wells, compared with that of the untreated wells (controls). The controls in the assays involved tests done with cells not incubated with the conjugate prodrugs. The experiments were performed in triplicate. IC_{50} was calculated with GraphPad Prism 5.[59,60]

Dark Toxicity Study. Cell plating was performed in a fashion similar to the phototoxicity study, but without illumination. Briefly, the media in each well was removed, rinsed three times with cold PBS, and replaced with fresh medium. The plates were kept in the dark for 30 min and then returned to the incubator. After an additional 72 h incubation, cell viability was determined using the MTT assay described above.

Impact of Excess Free FA in Culture Medium on the Cellular Uptake of Prodrug. In order to demonstrate that FA and FA-conjugates compete for the same receptors, 5 × 10^4 colon 26 cells in 96-well plates were preincubated with 1 mM FA (100-fold excess of free FA).[54] After 1 h, 10 μM of prodrugs **3**, **4**, or **5** was added. At the end of each incubation period, fluorescence emission was taken as indicated in the uptake

experiment. Briefly, colon 26 cells were incubated in 96-well plates at a cell density of 5×10^4 cells per well in complete medium for 24 h. 5 mM FA was prepared by first dissolving an appropriate amount of the compound in 1 mL DMSO at 60 °C, and later diluting it in PBS to make a total volume of 10 mL. 26.6 μL of this solution was then added to 133 μL of complete medium in the well plate to achieve a 1 mM free FA. This was incubated for 1 h before the addition of 40 μL of prodrug in complete media solution. At various time points, the fluorescence of wells with free FA was measured, following the same protocol as the uptake experiment. The results were compared with wells without free FA at the same time points. The results are expressed as fluorescence units within a given volume of solvent.

In Vivo Optical Imaging. Three 4-to-6-week-old female Balb/c mice (~20−22 g, Charles Rivers Laboratories, Inc.) were used to monitor the distribution and tumor targeting ability of the five prodrugs. The mice were implanted subcutaneously with 2×10^6 colon 26 cells in PBS (100 μL) on the lower back neck. Tumor growth was monitored with digital calipers for 14 days, until the tumors reached 4−6 mm in diameter. The mice were then anesthetized in an acrylic chamber with a 2.5% isoflurane/air mixture followed by retro-orbital injection with 2 μmol/kg of the prodrugs in 5% Cremophor solutions (PBS/EtOH/Cremophor, 18:1:1 v/v/v) . Images were taken using the IVIS imaging system (Caliper Life Sciences), which consisted of a cryogenically cooled imaging system coupled to the data acquisition computer running Living Image software. Fluorescence images were taken at 0, 0.25, 1, 3, 7, 9, 24, 48, and 72 h postinjection. During the imaging process, the following parameters were used: fluorescence mode, exposure time 0.5 s, binning: medium, F/Stop: 2, excitation: 675 filter (660−690 nm), and emission: 720 filter (710−730 nm). The mice were anesthetized before imaging. During post processing, image counts were adjusted to 11 000 A.U. as minimum and 30 000 A.U. as maximum color scale.

Tissue Distribution. Tumor-bearing mice (20−23 g) were randomly divided into two groups (n = 3 mice per group). Four μmol/kg of prodrug **4** or **5** in 5% Cremophor formulation (200 μL) were administered via retro-orbital injection into each animal. [For the study with the excess FA, FA (200 μmol/kg) in 0.2 mL saline was IP-injected to mice 1.5 h before the prodrug injection.] At 7 h post injection, all mice were euthanized by CO_2 inhalation and exsanguinated by opening the thoracic cavity. Blood samples were withdrawn from the heart through a syringe and immediately centrifuged at 1200 rpm for 10 min to collect the plasma. Tissues were excised from major organs (lungs, heart, kidneys, muscle, liver, skin, spleen), rinsed with PBS, and blotted dry with absorbent tissue. 150 mg of excised tissues in 1 mL DMSO was homogenized for 2 min. The homogenates were centrifuged at 12 000 rpm for 10 min. The supernatants were then pipetted into three wells of a 96-well plate.150 mg of blood plasma was weighed out, diluted with 1 mL DMSO, and treated like the other tissues. The fluorescence was read using a microplate reader with excitation wavelengths at 605 nm and emission wavelengths of 640−800 nm. The uptake to the tissues was reported as the mean fluorescence unit and standard deviation. The 7 h time point was selected based on the in vivo life imaging data, when prodrug **4** has a maximum tumor/skin ratio.

Treatment of Mice with SC Colon 26 Tumors. All animals were 4 to 6 weeks old at the time of injection. A total of 2×10^6 colon 26 cells in 100 μL PBS were implanted subcutaneously on the lower back of the neck. Tumor volumes were monitored with digital calipers and calculated as an ellipsoid volume using the formula $(\pi/2)lw^2$, where l = longest axis of tumor and w = shortest axis perpendicular to l. Mice with tumors 4−6 mm in diameter were used for the experiment. 4 mM DMSO stock solutions of prodrug **4** or **5** were diluted to achieve final a concentration of 2 μmol/kg with 5% Cremophor formulation. 200 μL of the sample via retro-orbital injection was administered once on day 0. Seven hours after injection, the mice were anaesthetized via ketamine 80 mg/kg and xylazine 6 mg/kg injected IP. The tumor area was then illuminated for 30 min with a 690 nm diode laser at 100 mW/cm^2 (180 J/cm^2). Tumor size was measured every 2 days. Three groups (n = 3 mice per group) were tested: (1) control (without conjugates or irradiation), (2) 2 μmol/kg prodrug **4** + $h\nu$, and (3) 2 μmol/kg prodrug **5** + $h\nu$.

■ ASSOCIATED CONTENT

Ⓢ Supporting Information

Synthetic schemes of compounds **13** and 17; UV−vis absorption spectral data; a graph of changes in body weight during the treatment; dark toxicity; and characterization and purity data (^{1}H NMR, ^{13}C NMR, MS, HPLC). This material is available free of charge via the Internet at http://pubs.acs.org.

■ AUTHOR INFORMATION

Corresponding Author

*E-mail: youngjae-you@ouhsc.edu. Tel.: 1-405-271-6593, ext. 47473. Fax: 1-405-271-7505.

Notes

The authors declare no competing financial interest.

■ ACKNOWLEDGMENTS

We appreciate the helpful discussions with Dr. Sukyung Woo. We thank the Peggy and Charles Stephenson Cancer Center at the University of Oklahoma Health Sciences Center, Oklahoma City, OK, and an Institutional Development Award (IDeA) from the National Institute of General Medical Sciences of the National Institutes of Health under grant number P20 GM103639 for the use of the Molecular Imaging Core facility that provided services for the optical in vivo imaging. This research was supported by the DoD [Breast Cancer Research Program] under Award Number W81XWH-09-1-0071 and the office of Vice President of Research at OUHSC. Views and opinions of and endorsements by the authors do not reflect those of the U.S. Army or the DoD.

■ ABBREVIATIONS

CA4, combretastatin A-4; CMP, core-modified porphyrin; D, drug; DCC, *N,N′*-dicyclohexylcarbodiimide; DIPEA, *N,N*-diisopropylethylamine; FR, folate receptor; FA, folic acid; HBTU, (*1H*-benzotriazol-1-yloxy)(dimethylamino)-*N,N*-dimethylmethaniminium hexafluorophosphate; L, singlet oxygen-cleavable linker; NCL, noncleavable linker; Pc, phthalocyanine; PDT, photodynamic therapy; PMDETA, *N,N,N′,N″,N″*-pentamethyldiethylenetriamine; fPS, fluorescent photosensitizer; SO, singlet oxygen; sp, spacer

REFERENCES

(1) Andresen, T. L., Jensen, S. S., and Jorgensen, K. (2005) Advanced strategies in liposomal cancer therapy: problems and prospects of active and tumor specific drug release. *Prog. Lipid Res. 44*, 68−97.

(2) Alvarez-Lorenzo, C., and Concheiro, A. (2014) Smart drug delivery systems: from fundamentals to the clinic. *Chem. Commun. 50*, 7743−7765.

(3) Langer, R. (1998) Drug delivery and targeting. *Nature 392*, 5−10.

(4) Chabner, B. A., and Roberts, T. G., Jr. (2005) Timeline: Chemotherapy and the war on cancer. *Nat. Rev. Cancer 5*, 65−72.

(5) Pytel, D., Sliwinski, T., Poplawski, T., Ferriola, D., and Majsterek, I. (2009) Tyrosine kinase blockers: new hope for successful cancer therapy. *Anticancer Agents Med. Chem. 9*, 66−76.

(6) Druker, B. J., Tamura, S., Buchdunger, E., Ohno, S., Segal, G. M., Fanning, S., Zimmermann, J., and Lydon, N. B. (1996) Effects of a selective inhibitor of the Abl tyrosine kinase on the growth of Bcr-Abl positive cells. *Nat. Med. 2*, 561−566.

(7) Schrama, D., Reisfeld, R. A., and Becker, J. C. (2006) Antibody targeted drugs as cancer therapeutics. *Nat. Rev. Drug Discovery 5*, 147−159.

(8) Sievers, E. L., and Senter, P. D. (2013) Antibody-drug conjugates in cancer therapy. *Annu. Rev. Med. 64*, 15−29.

(9) Xia, W., and Low, P. S. (2010) Folate-targeted therapies for cancer. *J. Med. Chem. 53*, 6811−6824.

(10) Carpenter, R. D., Andrei, M., Aina, O. H., Lau, E. Y., Lightstone, F. C., Liu, R., Lam, K. S., and Kurth, M. J. (2009) Selectively targeting T- and B-cell lymphomas: a benzothiazole antagonist of alpha4beta1 integrin. *J. Med. Chem. 52*, 14−19.

(11) Garanger, E., Boturyn, D., and Dumy, P. (2007) Tumor targeting with RGD peptide ligands-design of new molecular conjugates for imaging and therapy of cancers. *Anticancer Agents Med. Chem. 7*, 552−558.

(12) Gupta, Y., Kohli, D. V., and Jain, S. K. (2008) Vitamin B12-mediated transport: a potential tool for tumor targeting of antineoplastic drugs and imaging agents. *Crit. Rev. Ther. Drug Carrier Syst. 25*, 347−379.

(13) Low, P. S., and Kularatne, S. A. (2009) Folate-targeted therapeutic and imaging agents for cancer. *Curr. Opin. Chem. Biol. 13*, 256−262.

(14) Irache, J. M., Salman, H. H., Gamazo, C., and Espuelas, S. (2008) Mannose-targeted systems for the delivery of therapeutics. *Expert Opin. Drug Delivery 5*, 703−724.

(15) Lee, R. J., Wang, S., and Low, P. S. (1996) Measurement of endosome pH following folate receptor-mediated endocytosis. *Biochim. Biophys. Acta 1312*, 237−242.

(16) Yang, J., Chen, H., Vlahov, I. R., Cheng, J. X., and Low, P. S. (2006) Evaluation of disulfide reduction during receptor-mediated endocytosis by using FRET imaging. *Proc. Natl. Acad. Sci. U.S.A. 103*, 13872−13877.

(17) Alvarez-Lorenzo, C., Bromberg, L., and Concheiro, A. (2009) Light-sensitive intelligent drug delivery systems. *Photochem. Photobiol. 85*, 848−860.

(18) Bio, M., Nkepang, G., and You, Y. (2012) Click and photo-unclick chemistry of aminoacrylate for visible light-triggered drug release. *Chem. Commun. 48*, 6517−6519.

(19) Bio, M., Rajaputra, P., Nkepang, G., Awuah, S. G., Hossion, A. M., and You, Y. (2013) Site-specific and far-red-light-activatable prodrug of combretastatin A-4 using photo-unclick chemistry. *J. Med. Chem. 56*, 3936−3942.

(20) Bio, M., Rajaputra, P., Nkepang, G., and You, Y. J. (2014) Far-red light activatable, multifunctional prodrug for fluorescence optical imaging and combinational treatment. *J. Med. Chem. 57*, 3401−3409.

(21) Hossion, A. M. L., Bio, M., Nkepang, G., Awuah, S. G., and You, Y. (2013) Visible light controlled release of anticancer drug through double activation of prodrug. *ACS Med. Chem. Lett. 4*, 124−127.

(22) Jiang, M. Y., and Dolphin, D. (2008) Site-specific prodrug release using visible light. *J. Am. Chem. Soc. 130*, 4236−42367.

(23) Lee, J., Park, J., Singha, K., and Kim, W. J. (2013) Mesoporous silica nanoparticle facilitated drug release through cascade photosensitizer activation and cleavage of singlet oxygen sensitive linker. *Chem. Commun. 49*, 1545−1547.

(24) Mahendran, A., Kopkalli, Y., Ghosh, G., Ghogare, A., Minnis, M., Kruft, B. I., Zamadar, M., Aebisher, D., Davenport, L., and Greer, A. (2011) A hand-held fiber-optic implement for the site-specific delivery of photosensitizer and singlet oxygen. *Photochem. Photobiol. 87*, 1330−1337.

(25) Murthy, R. S., Bio, M., and You, Y. J. (2009) Low energy light-triggered oxidative cleavage of olefins. *Tetrahedron Lett. 50*, 1041−1044.

(26) Nkepang, G., Pogula, P. K., Bio, M., and You, Y. J. (2012) Synthesis and singlet oxygen reactivity of 1,2-diaryloxyethenes and selected sulfur and nitrogen analogs. *Photochem. Photobiol. 88*, 753−759.

(27) Ruebner, A., Yang, Z. W., Leung, D., and Breslow, R. (1999) A cyclodextrin dimer with a photocleavable linker as a possible carrier for the photosensitizer in photodynamic tumor therapy. *Proc. Natl. Acad. Sci. U.S.A. 96*, 14692−14693.

(28) Zamadar, M., Ghosh, G., Mahendran, A., Minnis, M., Kruft, B. I., Ghogare, A., Aebisher, D., and Greer, A. (2011) Photosensitizer drug delivery via an optical fiber. *J. Am. Chem. Soc. 133*, 7882−7891.

(29) Bartusik, D., Aebisher, D., Ghogare, A., Ghosh, G., Abramova, I., Hasan, T., and Greer, A. (2013) A fiberoptic (photodynamic therapy type) device with a photosensitizer and singlet oxygen delivery probe tip for ovarian cancer cell killing. *Photochem. Photobiol. 89*, 936−941.

(30) Chakraborty, A., Held, K. D., Prise, K. M., Liber, H. L., and Redmond, R. W. (2009) Bystander effects induced by diffusing mediators after photodynamic stress. *Radiat. Res. 172*, 74−81.

(31) Rubio, N., Rajadurai, A., Held, K. D., Prise, K. M., Liber, H. L., and Redmond, R. W. (2009) Real-time imaging of novel spatial and temporal responses to photodynamic stress. *Free Radic. Biol. Med. 47*, 283−290.

(32) Leamon, C. P. (2008) Folate-targeted drug strategies for the treatment of cancer. *Curr. Opin. Invest. Drugs 9*, 1277−1286.

(33) Vlahov, I. R., and Leamon, C. P. (2012) Engineering folate-drug conjugates to target cancer: from chemistry to clinic. *Bioconjugate Chem. 23*, 1357−1369.

(34) Chen, C., Ke, J., Zhou, X. E., Yi, W., Brunzelle, J. S., Li, J., Yong, E. L., Xu, H. E., and Melcher, K. (2013) Structural basis for molecular recognition of folic acid by folate receptors. *Nature 500*, 486−489.

(35) Westerhof, G. R., Schornagel, J. H., Kathmann, I., Jackman, A. L., Rosowsky, A., Forsch, R. A., Hynes, J. B., Boyle, F. T., Peters, G. J., Pinedo, H. M., et al. (1995) Carrier- and receptor-mediated transport of folate antagonists targeting folate-dependent enzymes: correlates of molecular-structure and biological activity. *Mol. Pharmacol. 48*, 459−471.

(36) Leamon, C. P., You, F., Santhapuram, H. K., Fan, M. J., and Vlahov, I. R. (2009) Properties influencing the relative binding affinity of pteroate derivatives and drug conjugates thereof to the folate receptor. *Pharm. Res. 26*, 1315−1323.

(37) Zhao, X. B., Li, H., and Lee, R. J. (2008) Targeted drug delivery via folate receptors. *Expert Opin. Drug Delivery 5*, 309−319.

(38) Salazar, M. D., and Ratnam, M. (2007) The folate receptor: What does it promise in tissue-targeted therapeutics? *Cancer Metast. Rev. 26*, 141−152.

(39) Low, P. S., Henne, W. A., and Doorneweerd, D. D. (2008) Discovery and development of folic-acid-based receptor targeting for imaging and therapy of cancer and inflammatory diseases. *Acc. Chem. Res. 41*, 120−129.

(40) Leamon, C. P., Reddy, J. A., Vlahov, I. R., Westrick, E., Parker, N., Nicoson, J. S., and Vetzel, M. (2007) Comparative preclinical activity of the folate-targeted Vinca alkaloid conjugates EC140 and EC145. *Int. J. Cancer 121*, 1585−1592.

(41) Ladino, C. A., Chari, R. V., Bourret, L. A., Kedersha, N. L., and Goldmacher, V. S. (1997) Folate-maytansinoids: target-selective drugs of low molecular weight. *Int. J. Cancer 73*, 859−864.

(42) Leamon, C. P., Reddy, J. A., Vetzel, M., Dorton, R., Westrick, E., Parker, N., Wang, Y., and Vlahov, I. (2008) Folate targeting enables

durable and specific antitumor responses from a therapeutically null tubulysin B analogue. *Cancer Res. 68*, 9839−9844.
(43) Liu, T. W., Chen, J., Burgess, L., Cao, W., Shi, J., Wilson, B. C., and Zheng, G. (2011) Multimodal bacteriochlorophyll theranostic agent. *Theranostics 1*, 354−362.
(44) Shi, J., Liu, T. W., Chen, J., Green, D., Jaffray, D., Wilson, B. C., Wang, F., and Zheng, G. (2011) Transforming a targeted porphyrin theranostic agent into a PET imaging probe for cancer. *Theranostics 1*, 363−370.
(45) Greenwald, R. B., Choe, Y. H., McGuire, J., and Conover, C. D. (2003) Effective drug delivery by PEGylated drug conjugates. *Adv. Drug Delivery Rev. 55*, 217−250.
(46) Veronese, F. M., and Pasut, G. (2005) PEGylation, successful approach to drug delivery. *Drug Discovery Today 10*, 1451−1458.
(47) Duncan, R. (2003) The dawning era of polymer therapeutics. *Nat. Rev. Drug Discovery 2*, 347−360.
(48) Ohguchi, Y., Kawano, K., Hattori, Y., and Maitani, Y. (2008) Selective delivery of folate-PEG-linked, nanoemulsion-loaded aclacinomycin A to KB nasopharyngeal cells and xenograft: effect of chain length and amount of folate-PEG linker. *J. Drug Target 16*, 660−667.
(49) Moret, F., Scheglmann, D., and Reddi, E. (2013) Folate-targeted PEGylated liposomes improve the selectivity of PDT with meta-tetra(hydroxyphenyl)chlorin (m-THPC). *Photochem. Photobiol. Sci. 12*, 823−834.
(50) Lee, R. J., and Low, P. S. (1994) Delivery of liposomes into cultured KB cells via folate receptor-mediated endocytosis. *J. Biol. Chem. 269*, 3198−3204.
(51) Gravier, J., Schneider, R., Frochot, C., Bastogne, T., Schmitt, F., Didelon, J., Guillemin, F., and Barberi-Heyob, M. (2008) Improvement of meta-tetra(hydroxyphenyl)chlorin-like photosensitizer selectivity with folate-based targeted delivery. synthesis and in vivo delivery studies. *J. Med. Chem. 51*, 3867−3877.
(52) Yamada, A., Taniguchi, Y., Kawano, K., Honda, T., Hattori, Y., and Maitani, Y. (2008) Design of folate-linked liposomal doxorubicin to its antitumor effect in mice. *Clin. Cancer Res. 14*, 8161−8168.
(53) Jiang, X. J., Yeung, S. L., Lo, P. C., Fong, W. P., and Ng, D. K. P. (2011) Phthalocyanine -polyamine conjugates as highly efficient photosensitizers for photodynamic therapy. *J. Med. Chem. 54*, 320−330.
(54) Russell-Jones, G., McTavish, K., McEwan, J., Rice, J., and Nowotnik, D. (2004) Vitamin-mediated targeting as a potential mechanism to increase drug uptake by tumours. *J. Inorg. Biochem. 98*, 1625−1633.
(55) Verdoes, M., Florea, B. I., Hillaert, U., Willems, L. I., van der Linden, W. A., Sae-Heng, M., Filippov, D. V., Kisselev, A. F., van der Marel, G. A., and Overkleeft, H. S. (2008) Azido-BODIPY acid reveals quantitative Staudinger-Bertozzi ligation in two-step activity-based proteasome profiling. *ChemBioChem 9*, 1735−1738.
(56) Ke, M. R., Yeung, S. L., Ng, D. K., Fong, W. P., and Lo, P. C. (2013) Preparation and in vitro photodynamic activities of folate-conjugated distyryl boron dipyrromethene based photosensitizers. *J. Med. Chem. 56*, 8475−8483.
(57) Guaragna, A., Chiaviello, A., Paolella, C., D'Alonzo, D., and Palumbo, G. (2012) Synthesis and evaluation of folate-based chlorambucil delivery systems for tumor-targeted chemotherapy. *Bioconjugate Chem. 23*, 84−96.
(58) Leo, A., Hansch, C., and Elkins, D. (1971) Partition coefficients and their uses. *Chem. Rev. 71*, 525−616.
(59) You, Y., Gibson, S. L., and Detty, M. R. (2006) Phototoxicity of a core-modified porphyrin and induction of apoptosis. *J. Photochem. Photobiol., B 85*, 155−162.
(60) You, Y., Gibson, S. L., Hilf, R., Ohulchanskyy, T. Y., and Detty, M. R. (2005) Core-modified porphyrins. Part 4: Steric effects on photophysical and biological properties in vitro. *Bioorg. Med. Chem. 13*, 2235−2251.